

Role of ceramic supports on microwave heating of materials

Tanmay Basak and A. Shanthi Priya

Citation: [Journal of Applied Physics](#) **97**, 083537 (2005); doi: 10.1063/1.1871356

View online: <http://dx.doi.org/10.1063/1.1871356>

View Table of Contents: <http://scitation.aip.org/content/aip/journal/jap/97/8?ver=pdfcov>

Published by the [AIP Publishing](#)

Articles you may be interested in

[Development of a compact cylindrical reaction cavity for a microwave dielectric heating system](#)

Rev. Sci. Instrum. **83**, 034703 (2012); 10.1063/1.3693344

[Electron-emission yield under electron impact of ceramics used as channel materials in Hall-effect thrusters](#)

J. Appl. Phys. **110**, 093301 (2011); 10.1063/1.3653820

[Role of ceramic matrix and Au fraction on the morphology and optical properties of cosputtered Au-ceramic thin films](#)

J. Appl. Phys. **101**, 113532 (2007); 10.1063/1.2745124

[Preferred orientation of pores in ceramics under heating by a linearly polarized microwave field](#)

J. Appl. Phys. **101**, 084915 (2007); 10.1063/1.2723187

[Theoretical analysis of the microwave-drill near-field localized heating effect](#)

J. Appl. Phys. **97**, 034909 (2005); 10.1063/1.1836011



Role of ceramic supports on microwave heating of materials

Tanmay Basak^{a)} and A. Shanthi Priya

Department of Chemical Engineering, Indian Institute of Technology, Madras, Chennai 600 036, India

(Received 1 November 2004; accepted 24 January 2005; published online 8 April 2005)

A detailed analysis has been carried out to study efficient heating due to microwaves for one-dimensional samples placed on ceramic supports (Al_2O_3 , SiC). The greater effects on microwave heating of samples have been illustrated via average power within a sample versus sample thickness diagram for various cases. The maxima in power, also termed as “resonances,” is observed for specific sample thicknesses and the two consecutive maxima in average power are termed as R_1 and R_2 modes. The greater heating effects leading to *hot spots* would occur in water samples during both-sides incidence when the sample is kept on Al_2O_3 support. SiC support may be recommended for water samples due to uniform heating throughout the sample. In contrast, SiC support could cause local hot spots or thermal runaway for oil samples. The localized hot spots are more pronounced for the samples exposed to microwaves on both faces. The choice of support may not be trivial due to the complex dielectric response of sample-support assembly. Current analysis has been illustrated for low- and high-dielectric materials (water and oil) and a representative case study has also been shown for beef samples. Based on such observations, a generalized heating strategy for materials due to uniform plane waves has been derived. © 2005 American Institute of Physics. [DOI: 10.1063/1.1871356]

I. INTRODUCTION

Electromagnetic radiations in the frequency range from 300 MHz to 300 GHz are known as microwaves (MWs) and the typical wavelengths of MWs are within a few millimeters to 30 cm. Unique applications of microwave heat processing are baking, cooking, curing, drying, enzyme inactivation, heating, precooking, thawing, tempering, and many more. During MW heating, the material dielectric loss which is a function of frequency of MWs is responsible to convert electric energy into heat. Dielectric response for various materials plays an important role to carry out efficient material processing and a significant amount of earlier research was devoted to understand the physics on microwave-assisted transport and heating characteristics.^{1–6} Maxima in average power or spatial maxima in power occurring for specific sample dimensions lead to greater rates of thermal processing. Some of these nontrivial and counterintuitive heating effects received significant attention based on enhanced thermal processing due to volumetric effects of MW propagation.

A detailed analysis on modeling of microwave heating has been carried out by Ayappa *et al.*^{5,6} and their investigations were based on heating of one-dimensional (1D) slabs and two-dimensional (2D) cylinders. They have done detailed theoretical analysis on coupled MW and heat transport for pure and multilayered slabs typically used in the food industry. Ayappa *et al.*⁵ analyzed the heating characteristics for multilayered food sandwich and nonuniform or local heating was observed for 1D bread-beef food slabs. The analysis was later extended for 2D samples due to transverse

electromagnetic (TEM) modes on heating and localized non-uniform heating was still observed for samples with specific radii.⁶

The localized or nonuniform heating in samples occur due to volumetric heating effects and considerable further studies were devoted on the analysis of maxima in power or “resonances” due to MW propagation. Ayappa *et al.*⁷ Ayappa,⁸ and Barringer *et al.*⁹ found the maxima in average power occurring only for the fixed sample dimension in 1D slabs and 2D cylinders. They also observed that the heating rates are considerably greater for those sample dimensions and the suitable relationships between the occurrence of resonance and the sample size were established. Microwave heating and transport models were further applied for thawing and heating of multiphase systems in recent investigations^{10–14} and greater rates in material processing were observed due to resonances. All these earlier works on heating and melting were carried out to investigate the heating effects solely due to the materials. Typically, materials are kept with a support in an oven or waveguide, and therefore, the foreign supporting materials may interfere with the heating strategies.

The suitable supports may be recommended as alumina (Al_2O_3) and SiC as they withstand high temperature, which may be the case during MW heating.¹⁵ In addition, ceramic supports also prevent typical food substances from corrosion. Heating characteristics and MW power absorption of ceramic materials show that Al_2O_3 absorbs much less power than SiC, resulting in greater temperature rise in SiC.¹⁵ The temperature profile within the ceramic materials is uniform due to higher thermal conductivity and these materials may be the perfect choice to be used as a support for various samples. Although Al_2O_3 support allows greater MW power to penetrate through, the coupled dielectric response of the

^{a)} Author to whom correspondence should be addressed; FAX: 91-44-2257-0509; electronic mail: tanmay@iitm.ac.in

sample-support assembly may not be trivial. The suitable choice of the support based on the dielectric properties of the sample would be important to carry out faster and/or uniform thermal material processing.

Current work attempts to analyze the efficient heating strategies in the presence of resonances or maxima in power within the sample. During resonances, a material absorbs greater power and the presence of a support may alter power absorption within a material. The resonating phenomena will be quite cumbersome for a material-ceramic composite and a detailed investigation on resonances for such material-ceramic systems has been carried out to achieve efficient heating strategies for material processing. We have analyzed the influence of supports for materials such as water, which is a highly lossy substance, and oil, with low dielectric loss, and these two limits would be useful to determine the heating strategies for other materials.

II. MODELING OF MICROWAVE TRANSPORT IN A MULTILAYERED SAMPLE

A. Electric field and power evaluations

We assume that the sample thickness is much smaller compared to the lateral dimensions and, hence, one-dimensional slab is a reasonable representation for the material-ceramics assembly. A similar modeling assumption can be found in earlier literatures.^{5,8,10,13-17} The wave propagation due to uniform electric field E_x , given by Maxwell's equation, is

$$\frac{d^2 E_x}{dz^2} + k^2 E_x = 0, \quad (1)$$

where E_x lies in the x - y plane and varies only in the direction of propagation, z axis (Fig. 1). In Eq. (1), $k = (\omega/c)\sqrt{\kappa' + i\kappa''}$ is the propagation constant which depends on the dielectric constant κ' and the dielectric loss κ'' ; $\omega = 2\pi f$, where f is the frequency of the electromagnetic wave, and c is the velocity of light. In an n -multilayered sample the electric field for the l th layer obtained from Eq. (1) is

$$\left. \begin{aligned} E_{t,l} e^{ik_l z_l} + E_{r,l} e^{-ik_l z_l} - E_{t,l+1} e^{ik_{l+1} z_l} - E_{r,l+1} e^{-ik_{l+1} z_l} \\ k_l E_{t,l} e^{ik_l z_l} - k_l E_{r,l} e^{-ik_l z_l} - k_{l+1} E_{t,l+1} e^{ik_{l+1} z_l} + k_{l+1} E_{r,l+1} e^{-ik_{l+1} z_l} \end{aligned} \right\} = 0 \quad l = 1 \dots n-1. \quad (5)$$

As the incident field intensities from the left and right are known, i.e., $E_{t,1} = E_L$ and $E_{r,n} = E_R$, Eqs. (5) are solved for the remaining $2n-2$ coefficients using MATLAB.^{13,14} For the l th layer, the transmitted and reflected waves are

$$E_{x,l}^t = E_{t,l} e^{ik_l z} = A_{x,l}^t e^{i\delta_{x,l}^t},$$

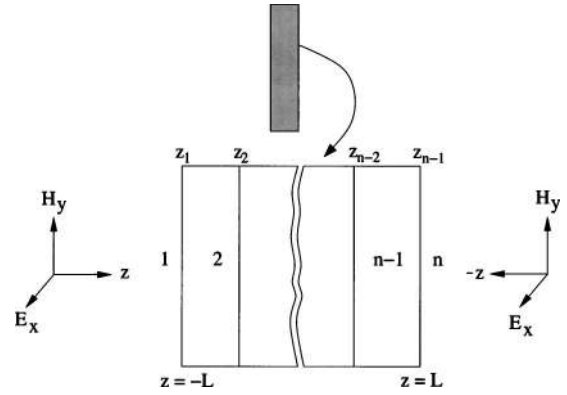


FIG. 1. Schematic illustration of a multilayered sample exposed to a plane electromagnetic wave.

$$\frac{d^2 E_{x,l}}{dz^2} + k_l^2 E_{x,l} = 0, \quad (2)$$

where $z_{l-1} \leq z \leq z_l$ and $l = 1 \dots n$. We assume each layer has constant dielectric properties and, hence, the general solution to Eq. (2) represented as a linear combination of transmitted and reflected waves propagating in opposite directions is

$$\begin{aligned} E_{x,1} &= E_{t,1} e^{ik_1 z} + E_{r,1} e^{-ik_1 z}, & \text{First layer} \\ E_{x,l} &= E_{t,l} e^{ik_l z} + E_{r,l} e^{-ik_l z}, & \text{Intermediate layers} \\ & l = 2 \dots n-1 \\ E_{x,n} &= E_{t,n} e^{ik_n z} + E_{r,n} e^{-ik_n z}, & \text{nth layer,} \end{aligned} \quad (3)$$

where $E_{t,l}$ and $E_{r,l}$ are the coefficients due to transmission and reflection, respectively. The boundary conditions at the interface are

$$\left. \begin{aligned} E_{x,l-1} &= E_{x,l} \\ \frac{dE_{x,l-1}}{dz} &= \frac{dE_{x,l}}{dz} \end{aligned} \right\} \begin{aligned} l &= 2 \dots n \\ z &= z_1 \dots z_{n-1} \end{aligned}. \quad (4)$$

Here z_1, z_2, \dots, z_{n-1} denote the boundaries between interfaces, as seen in Fig. 1.

The interface conditions [Eqs. (4)] and the general solutions [Eqs. (3)] are used to obtain the coefficients $E_{t,l}$ and $E_{r,l}$ via solving the set of algebraic equations

$$E_{x,l}^r = E_{r,l} e^{-ik_l z} = A_{x,l}^r e^{i\delta_{x,l}^r}, \quad (6)$$

where the corresponding amplitudes are given by

$$\begin{aligned} A_{x,l}^t &= \sqrt{E_{x,l}^t E_{x,l}^{t*}}, \\ A_{x,l}^r &= \sqrt{E_{x,l}^r E_{x,l}^{r*}}, \end{aligned} \quad (7)$$

and the phase states are given by

$$\delta_{x,l}^t = \tan^{-1} \left[\frac{\text{Im}(E_{x,l}^t)}{\text{Re}(E_{x,l}^t)} \right],$$

$$\delta_{x,l}^r = \tan^{-1} \left[\frac{\text{Im}(E_{x,l}^r)}{\text{Re}(E_{x,l}^r)} \right], \quad (8)$$

where the superscript “*” in Eq. (7) denotes the complex conjugate. For a stationary wave in the l th layer, the amplitude is given by

$$A_{x,l} = \sqrt{E_{x,l} E_{x,l}^*} \quad (9)$$

and the difference in phase angle is given by

$$\delta_{x,l} = \delta_{x,l}^t - \delta_{x,l}^r, \quad (10)$$

where the quantities $E_{x,l}$ and $E_{x,l}^*$ that appeared in Eq. (9) are evaluated using Eqs. (3) and (6). At the resonance, the difference in phase angle is zero, i.e., $\delta_{x,l} = 0$.

The absorbed power in the l th layer obtained from the Poynting vector theorem is

$$q_l(z) = \frac{1}{2} \omega \epsilon_0 \kappa'' E_{x,l}(z) E_{x,l}^*(z). \quad (11)$$

The average power obtained by integrating the power across the slab is

$$\bar{q} = \frac{1}{2L} \int_{-L}^{+L} q_l(z) dz \approx \frac{1}{n} \sum_{i=1}^n q_l(z_i). \quad (12)$$

Here $-L$ and L denote the left and right faces of the slab, respectively, $0 \leq z_i \leq 2L$, n denotes the total number of data set, and $q_l(z_i)$ denotes the power as a function of z_i where z_i may be measured from the left edge of the slab or sample. Note that $2L$ is the thickness of the entire slab consisting of sample and supports. We will denote L_s as the thickness of the sample and L' as the total thickness of the support such that $2L = L_s + L'$. The average power for a sample of thickness L_s is

$$q_{\text{av}} = \frac{1}{n} \sum_{i=1}^n q_l(z_i), \quad (13)$$

where $0 \leq z_i \leq L_s$.

B. Modeling of microwave heating and solution strategy

The energy balance equation due to the microwave-assisted heat source is

$$\rho c_p \frac{\partial T}{\partial t} = k \frac{\partial^2 T}{\partial z^2} + q(z), \quad (14)$$

where ρ is the density, c_p is the specific heat, k is the thermal conductivity and the volumetric heat source, $q(z)$ is defined in a similar manner as in Eq. (11). In an n -multilayered sample, the energy balance equation for the l th layer obtained from Eq. (14) is

$$(\rho c_p)_l \frac{\partial T_l}{\partial t} = k_l \frac{\partial^2 T_l}{\partial z^2} + q_l(z), \quad l = 1 \dots n. \quad (15)$$

The boundary conditions are

$$k_1 \frac{\partial T_1}{\partial z} = h(T_1 - T_\infty), \quad z = z_1 \quad (16)$$

and

$$-k_{n-1} \frac{\partial T_{n-1}}{\partial z} = h(T_{n-1} - T_\infty), \quad z = z_{n-1}. \quad (17)$$

The interface conditions between ceramic-material are

$$\left. \begin{aligned} T_l &= T_{l+1} \\ k_l \frac{\partial T_l}{\partial z} &= k_{l+1} \frac{\partial T_{l+1}}{\partial z} \end{aligned} \right\} \begin{aligned} l &= 2 \dots n-2 \\ z &= z_2 \dots z_{n-2} \end{aligned}. \quad (18)$$

The wave propagation equation for a particular medium (ceramic/material) is given in Eq. (2). As microwave power, $q_l(z)$ is a function of electric field as seen in Eq. (11) and, hence, a functional representation of the electric field is necessary to solve the energy balance equation [Eq. (15)]. The evaluation of the functional form of the electric field may be difficult for a multilayered sample, and we are unaware of such a solution till date. Alternatively, the energy balance and wave equations [Eqs. (2) and (15)] are solved numerically as discussed next.

Using the dimensionless variables,

$$u = \frac{E_x}{E_0}$$

and

$$\frac{d}{dz'} \equiv 2L \frac{d}{dz},$$

Eq. (1) reduces to

$$\frac{d^2 u}{dz'^2} + \gamma^2 u = 0, \quad (19)$$

where u is the electric-field intensity, $\gamma = (2L\omega/c) \sqrt{\kappa' + i\kappa''}$ is the propagation constant, and $2L$ is the thickness of the slab. Substituting the complex field variable $u = v + iw$ into Eq. (19) and equating the real and imaginary components, we get

$$\frac{d^2 v}{dz'^2} + \chi_1 v - \chi_2 w = 0 \quad (20)$$

and

$$\frac{d^2 w}{dz'^2} + \chi_2 v + \chi_1 w = 0, \quad (21)$$

with $\chi_1 = (4L^2 \omega^2 / c^2) \kappa'$ and $\chi_2 = (4L^2 \omega^2 / c^2) \kappa''$. The boundary conditions for the real and imaginary components are⁵

TABLE I. The thermal and dielectric properties are given for water, oil, raw beef, Al₂O₃, and SiC (Refs. 5,13,15).

Material property	Water	Oil	Raw beef	Al ₂ O ₃	SiC
Heat capacity, C_p (J kg ⁻¹ °K ⁻¹)	4190	2000	2510	1046	3300
Thermal conductivity, k (W m ⁻¹ °K ⁻¹)	0.609	0.168	0.491	26	40
Density, ρ (kg m ⁻³)	1000	900	1070	3750	3100
Dielectric constant (2450 MHz), κ'	78.1	2.8	43	10.8	26.66
Dielectric loss (2450 MHz), κ''	10.44	0.15	15	0.1566	27.99

$$\left. \begin{aligned} \frac{dv}{dz'} - \frac{2\omega L}{c}w &= \frac{4\omega L}{c}\sin\left(\frac{\omega L}{c}\right) \\ \frac{dw}{dz'} + \frac{2\omega L}{c}v &= \frac{4\omega L}{c}\cos\left(\frac{\omega L}{c}\right) \end{aligned} \right\} \text{ at } z' = 0 \quad (22)$$

and

$$\left. \begin{aligned} \frac{dv}{dz'} + \frac{2\omega L}{c}w &= -\frac{E_R 4\omega L}{E_L c}\sin\left(\frac{\omega L}{c}\right) \\ \frac{dw}{dz'} - \frac{2\omega L}{c}v &= -\frac{E_R 4\omega L}{E_L c}\cos\left(\frac{\omega L}{c}\right) \end{aligned} \right\} \text{ at } z' = 1. \quad (23)$$

The dimensionless form of the energy balance equation in the presence of microwave, Eq. (14) is

$$\overline{(\rho c_p)_l} \frac{\partial \theta_l}{\partial \tau} = \overline{k_l} \frac{\partial^2 \theta_l}{\partial z'^2} + Q_l(z'), \quad (24)$$

where

$$\theta_l = \frac{T_l - T_\infty}{T_0}, \quad \overline{(\rho c_p)_l} = \frac{(\rho c_p)_l}{\rho_0 c_{p_0}}$$

and

$$\overline{k_l} = \frac{k_l}{k_0}.$$

Here T_0 denotes the initial temperature of the sample. The expression for the microwave power term in Eq. (24) is

$$Q_l(z') = \frac{2L^2 \omega \epsilon_0 \kappa'' E_0^2}{k_0 T_0} (v^2 + w^2). \quad (25)$$

The boundary conditions in dimensionless form, Eqs. (16) and (17), are

$$\frac{\partial \theta_1}{\partial z'} - Bi_1(\theta_1) = 0, \quad z' = 0 \quad (26)$$

and

$$\frac{\partial \theta_{n-1}}{\partial z'} + Bi_{n-1}(\theta_{n-1}) = 0, \quad z' = 1. \quad (27)$$

The initial condition used in the analysis is

$$\theta(\tau = 0) = \frac{T_0 - T_\infty}{T_0}, \quad \text{for } 0 \leq z' \leq 1. \quad (28)$$

The energy balance equation and the electric-field equations with the appropriate boundary conditions are solved using Galerkin finite element method. The interface conditions for the energy balance and electric-field equations due

to multiple phases are automatically satisfied via an interface element common to two phases. At the interface node, the field variable and fluxes are continuous as discussed by Reddy¹⁸ and Ayappa *et al.*⁵ To discretize the time domain, the Crank–Nicholson method is used, and the nonlinear residual equations are solved using a Newton–Raphson method.^{5,10,13}

For all computations, the dielectric and thermal properties are obtained from Table I. Note that dielectric properties correspond to a MW frequency of 2450 MHz. In all cases, the sample is exposed to the MW radiation of intensity 3 W cm⁻² and heat transfer coefficient at the outer faces is maintained at 2 W m⁻² K⁻¹. The temperature of the sample and the support is 300 K at $t=0$ s. Analysis will be carried out for MWs incident on one face and on both faces.

III. RESULTS AND DISCUSSION

A. Average power absorption: Materials versus supports

We have carried out detailed analysis on microwave power and temperature distributions for water (high dielectric loss), oil (low dielectric loss), and raw beef. We will illustrate the influence of ceramic supports such as Al₂O₃ and SiC on MW power and thermal characteristics for various substances in the presence of resonances.

The resonances can be best illustrated by maxima in average power versus sample thickness diagram. We will carry out our case studies for resonances to illustrate the influence of ceramic supports. The significant resonances occur at two consecutive R_1 and R_2 modes and the average power at R_1 mode is generally greater than that at R_2 mode.

Figure 2 illustrates the average power distributions with ceramic supports and without any support when the samples are incident on one face only. During one-side incidence, the average power for a sample without any support exhibits maxima at $L_s = 0.5\lambda_m$ and λ_m during R_1 and R_2 modes, respectively. Note that the wavelengths (λ_m) for the water, oil, and raw beef samples are 1.38, 7.3, and 1.84 cm, respectively.

The efficient heating due to MWs may be either at R_1 or R_2 mode and the occurrence of the maxima corresponding to a sample thickness is dependent on the support for various materials (as seen in Fig. 2). Note that the circles indicate R_1 mode and the boxes indicate R_2 mode in Fig. 2. We have assumed a thickness of the support being 0.2 cm for all test cases. Note that Al₂O₃ is a transparent medium and SiC absorbs MWs significantly.¹⁵ Therefore, we assumed a smaller

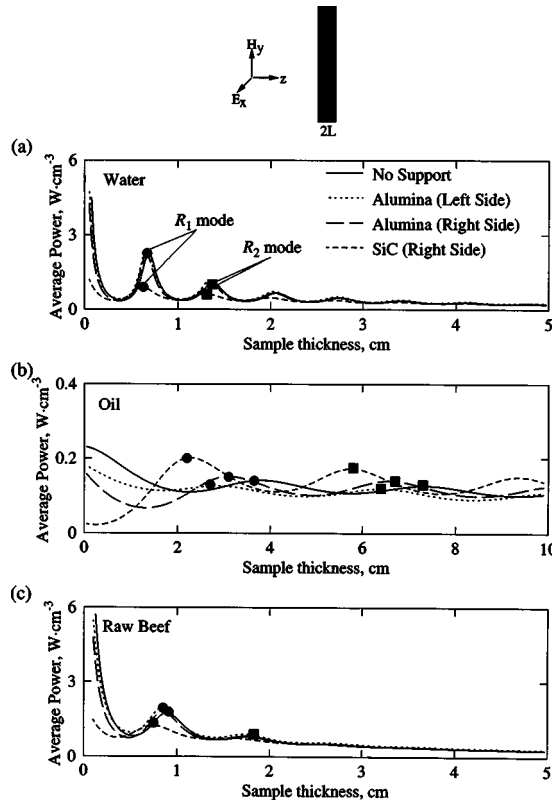


FIG. 2. Average power (q_{av} , $W\text{ cm}^{-3}$) vs sample thickness (L_s , cm) for (a) water, (b) oil, and (c) raw beef samples exposed to microwaves on one face. The filled circle denotes R_1 mode and the filled rectangle denotes R_2 mode of resonances.

thickness of the support and the influence of various thicknesses of the support on microwave heating of materials may not be important for current work. The average power versus sample thickness diagram for water indicates that the occurrence of R_1 and R_2 modes corresponding to specific sample thicknesses is almost unaffected by the presence of supports except that the less MW power deposition occurs within a sample with SiC supports [Fig. 2(a)]. It is interesting to note that the smaller average power versus sample thicknesses is observed with SiC support. A detailed investigation on the suitability of supports will be analyzed later to address the thermal runaway and efficient heating for various materials.

The average power versus sample thickness diagram for oil [Fig. 2(b)] indicates that the occurrence of R_1 and R_2 modes corresponding to specific sample thicknesses is significantly influenced by the presence of supports and the sample thicknesses corresponding to R_1 and R_2 modes are shifted, which are in contrast with the water samples. It is interesting to note that both the resonances (R_1, R_2) occur at smaller thickness with supports for oil samples. In addition, we observe that the oil samples with smaller thickness can absorb greater power with SiC supports as seen in Fig. 2(b). Figure 2(c) illustrates the average power distributions for raw beef and it is observed that similar to water, the occurrence of resonances is almost unaffected by the presence of supports and also a less MW power deposition is observed due to SiC support at the unexposed end.

Figure 3 illustrates the average power versus sample thickness for the samples with both-sides incidence. The av-

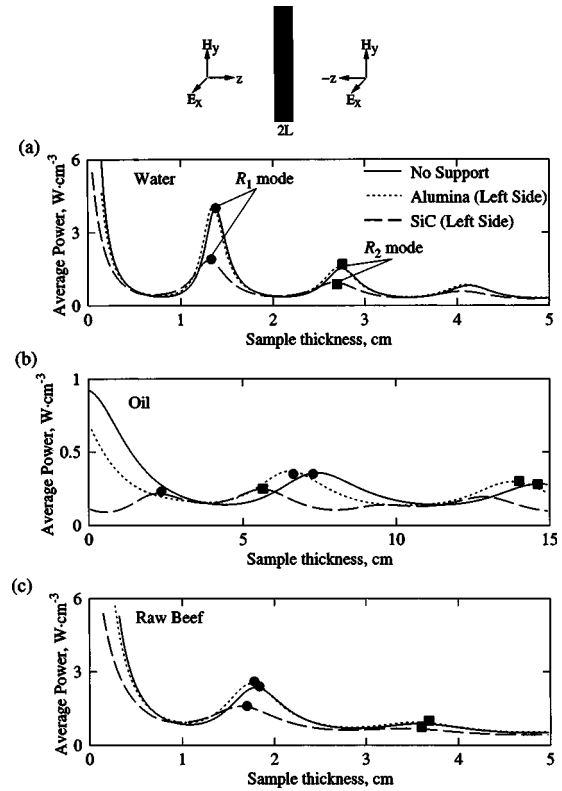


FIG. 3. Average power (q_{av} , $W\text{ cm}^{-3}$) vs sample thickness (L_s , cm) for (a) water, (b) oil, and (c) raw beef samples exposed to microwaves on both faces.

erage power distributions are qualitatively similar to one-side incidence cases, as seen in Fig. 2. For both-sides incidence, the sample thicknesses corresponding to resonances for all cases are greater than that due to one-side incidence. In addition, for oil samples, the resonances occur at much smaller thicknesses with SiC supports, as seen in Fig. 3(b).

The efficient use of supports depends on factors such as faster thermal processing, controlled or uniform thermal processing, selective heating, and many others. The interesting features as seen in Figs. 2 and 3 for various cases thus provide a stimulus for determining the role of the support on efficient heating due to MWs. The detailed analysis on MW power characteristics and electric-field distribution at various resonance modes would be useful to understand the interference of waves and the critical role of the specific ceramic support.

B. Microwave power and temperature distributions for water samples

Figure 4 illustrates the amplitude, power, and temperature distributions for the water sample during R_1 mode due to one-side incidence. For all the cases with and without supports, we study the MW power and field distribution for a fixed sample thickness ($L_s = 0.69$ cm) as the occurrence of the R_1 mode corresponds to the same sample thickness, as seen in Fig. 2(a). As seen in Fig. 4, for all cases, the amplitude of the transmitted wave is a decreasing function of the distance, whereas the amplitude of the reflected wave is an increasing function of the distance within the sample. It is

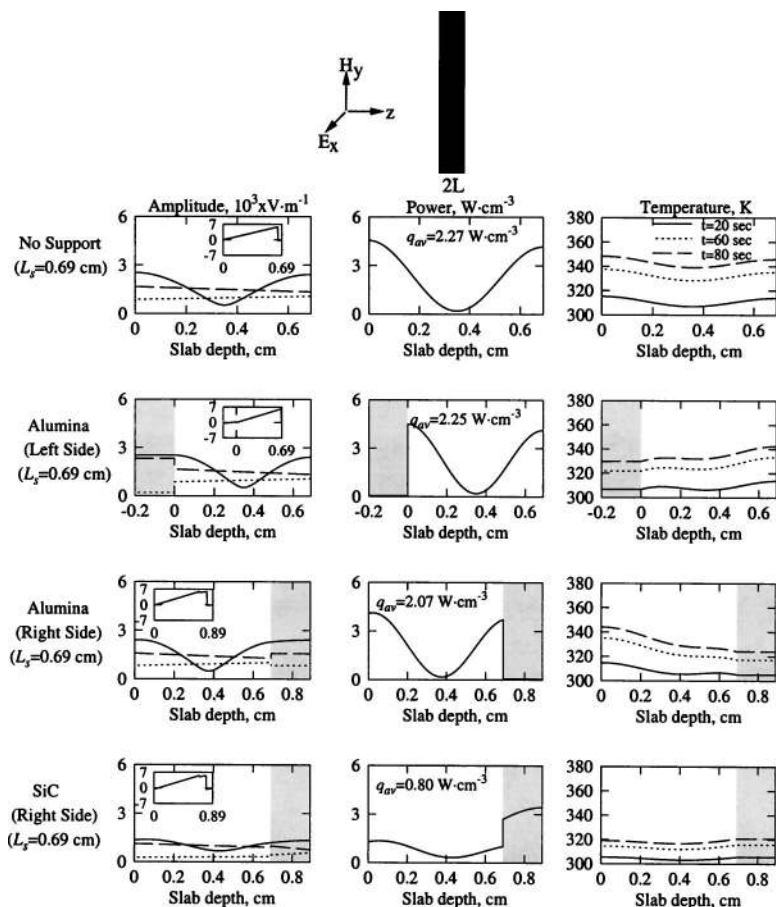


FIG. 4. Amplitudes of electric field ($A_{x,i}$, $A'_{x,i}$, $A''_{x,i}$), power distributions, and temperature profiles for water samples exposed to microwaves from the left face during R_1 mode. The ceramic support thickness = 0.2 cm, - - -, transmitted wave; ..., reflected wave; —, stationary wave. The shaded regime denotes the ceramic support. The inset shows phase difference ($\delta_{x,z}$) vs z .

interesting to note that there is a significant jump in the amplitudes of the transmitted wave and reflected waves within Al_2O_3 supports. The amplitude of the reflected wave is smaller than that of the transmitted wave, signifying smaller standing waves being formed within the support. In addition, due to the smaller dielectric loss of the Al_2O_3 support, the MW power absorption is quite small within the sample. Therefore, Al_2O_3 supports can be efficiently used due to the less power consumption.

The role of SiC support may be illustrated with a fact that more transmission and reflection within the support may decrease the amplitudes of traveling waves within the sample. Therefore, SiC support is preferred to be kept at the unexposed face of the sample. As seen in insets, the difference in phase angles versus distance within the slabs illustrates the strength of stationary waves and zero phase difference signifies the constructive interference, which is also termed as resonances. The resonances or maxima in power occur on both faces of the sample except the samples with SiC support, which correspond to a smaller power deposition at the unexposed end attached with SiC. The power absorption versus distance plot justifies that the average power absorbed by the sample is almost unaffected by the presence of Al_2O_3 , whereas the SiC layer absorbs greater power resulting in less microwave power absorption within a material. Note that the average power absorption within a sample with Al_2O_3 support at the right face is around 2.07 W cm^{-3} , whereas the average power is only 0.80 W cm^{-3} for samples with SiC supports.

The temperature distributions within the samples are illustrated by spatial temperature versus sample thickness diagram, as seen in Fig. 4. Here the temperatures are shown at 20, 60, and 80 s. During 80 s, the temperature varies within 340–348 K for the samples without support, and the temperature is within 324–342 K for samples with Al_2O_3 support at left/right side. Note that the location of the Al_2O_3 support either at the left or right side does not influence much the heating rate, as seen in Fig. 4, however, greater average power is observed for the samples with Al_2O_3 support at the left side. The heating rate of the sample is uniform with SiC supports due to lower power deposition throughout the sample, as seen in Fig. 4, and the temperature varies within 318–320 K. Although the temperature variation is smaller, SiC support could be useful to avoid *hot spots* for highly lossy substances like water. We have also carried out studies for R_2 mode (figures are not shown) and, similar to R_1 mode, the heating rate of the sample is uniform with SiC supports due to lower power deposition throughout the sample.

Figure 5 illustrates the amplitude, power, and temperature distributions for the water sample during R_1 mode due to both-sides incidence. As the samples are exposed on both faces, the transmitted and reflected waves are symmetric with each other within the sample, signifying more standing waves being formed. This leads to more power absorption in the sample than the one-side incidence case. The spatial distributions of the amplitude of traveling waves within the supports are qualitatively similar to that of the one-side inci-

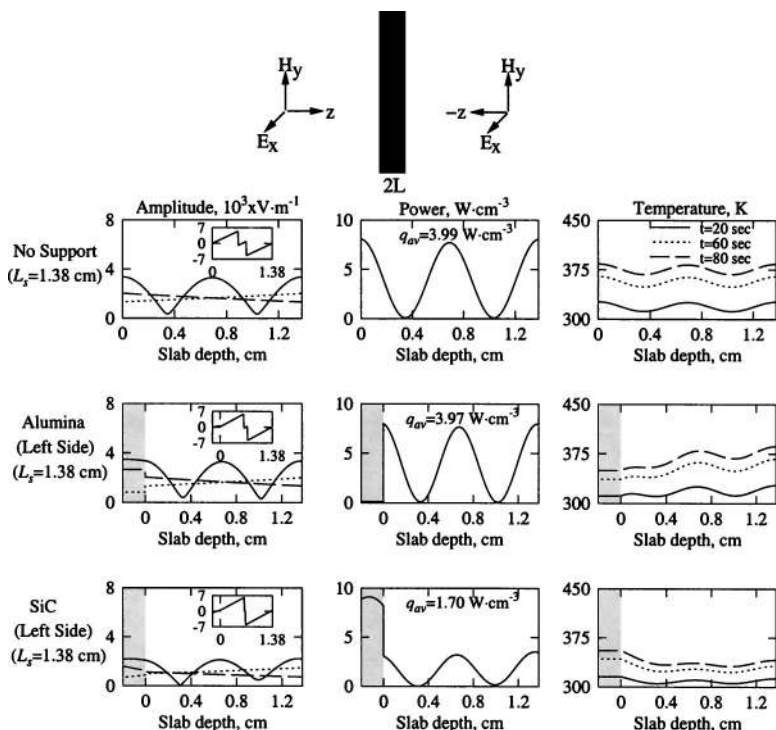


FIG. 5. Amplitudes of electric field ($A_{x,l}$, $A_{x,l}^i$, $A_{x,l}^r$), power distributions, and temperature profiles for water samples exposed to microwaves on both faces during R_1 mode. The ceramic support thickness = 0.2 cm. — —, transmitted wave;, reflected wave; —, stationary wave. The shaded regime denotes the ceramic support. The inset shows phase difference ($\delta_{x,l}$) vs z .

dence case as seen in Fig. 4 and three maxima in spatial power occurs within the samples, as seen in Fig. 5. Similar to one-side incidences, the average power absorption is almost unaffected by the presence of Al_2O_3 and lower power depositions are observed within samples with SiC supports as SiC absorbs a significant amount of power, as seen in Fig. 5. Note that the average power absorption within a sample with Al_2O_3 support is around 3.97 W cm^{-3} , whereas the average power is only 1.70 W cm^{-3} for the samples with SiC supports. During 80 s, the temperature varies within 351–386 K for the samples with Al_2O_3 support, whereas the variation is within 341–355 K in samples with SiC supports.

As MWs are incident on both sides and the Al_2O_3 support does not absorb much power, the temperature rise on the left face is small and the heating rates on the other face are larger. Consequently, a high temperature leading to a runaway heating effect would occur at the other face which is not attached to the Al_2O_3 support. In contrast, the SiC support may act as a heat source due to greater power absorption. Therefore, the uniform and lower temperature distribution is observed within the sample as the less MW energy would penetrate through the sample. During R_2 mode, we found more power peaks with smaller magnitudes within the samples, and spatial power distributions are much smaller for samples with SiC supports (figures are not shown).

Figure 6 illustrates the distribution of average temperature versus time for water samples with various cases. Note that the slope of the average temperature versus time denotes the heating rate and the heating rate is directly proportional to the MW power absorption as the heat loss to the ambience is very small. Figure 6(a) illustrates the average temperature distributions for one-side incidence cases during R_1 and R_2 modes. During R_1 mode, the heating rate without support is greater than that with supports. Al_2O_3 supports reduce the rate by a small amount and the heating rate is much smaller

with SiC supports. During 80 s, the average temperature without support is 343 K, whereas the average temperature with Al_2O_3 support is around 334 K (for both left and right supports). In contrast, the average temperature with SiC support is around 318 K only. The heating rate during R_2 mode is not much influenced by the Al_2O_3 supports, and the SiC support reduces the rate by a smaller amount. During 80 s, the average temperature without support is 320 K and that with SiC support is 311 K. The temperature distributions during both-sides incidence case as seen in Fig. 6(b) are qualitatively similar to one-side incidence cases. Similar to one-side incidence cases, SiC supports reduce the heating rate significantly.

C. Microwave power and temperature distributions for oil samples

Figure 7 illustrates the amplitude, power, and temperature distributions for oil samples during R_1 mode for one-side incidence. The maxima in average power during R_1 and R_2 modes for oil samples do not occur at an identical sample thickness as seen in Fig. 2(b) and we will illustrate the MW power, fields, and temperature distributions for a fixed resonance mode with various sample thicknesses, as seen in Fig. 7. It is interesting to note that the amplitude of the reflected wave is more within the sample when the Al_2O_3 support is placed at the right side than that with the support placed at the left side. This signifies more standing waves being formed in the sample, resulting in greater power absorption. In addition, the larger sample thickness can be processed for samples with the Al_2O_3 support at the right side. We also observe that the oil samples with SiC supports with smaller thickness ($L_s=2.25 \text{ cm}$) absorb greater power, especially near the regime attached with the support. Note that the average power absorption within a sample without a support is

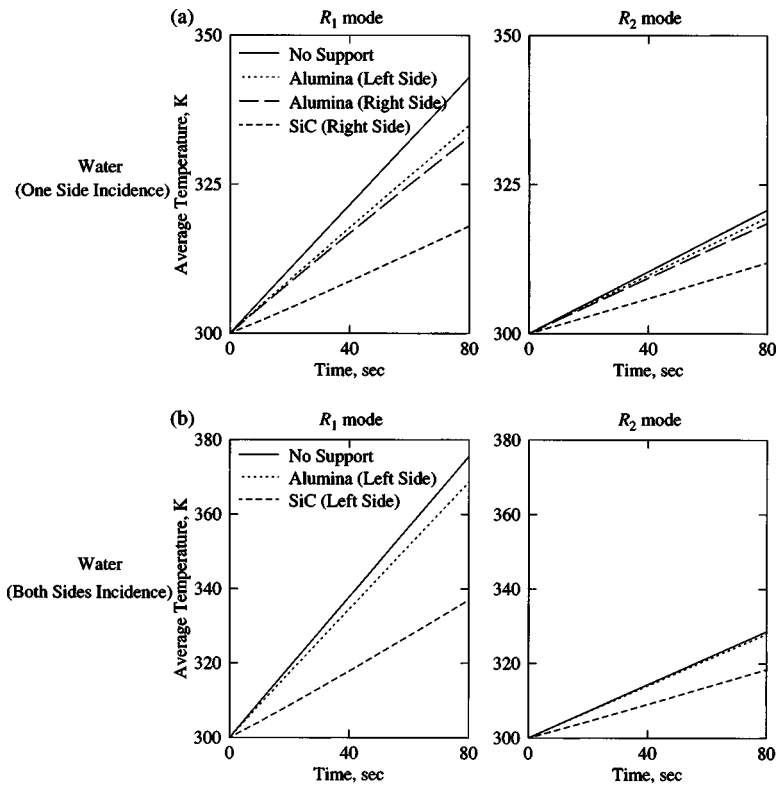


FIG. 6. Average temperature (K) vs sample thickness (cm) for water samples exposed to microwaves on (a) one face and (b) both faces during R_1 and R_2 modes.

around 0.14 W cm^{-3} , whereas the average power is around 0.15 W cm^{-3} for samples with Al_2O_3 support at the right side and that with SiC support is 0.20 W cm^{-3} .

The temperature distributions within the samples are illustrated by spatial temperature versus sample thickness dia-

gram, as seen in Fig. 7. Here the temperatures are shown at 20, 60, and 80 s. Note that the location of the Al_2O_3 support either at the left or right side does not influence much the heating rate, as seen in Fig. 7. The SiC support acts as a heat source and can be used for localized or surface heating. Dur-

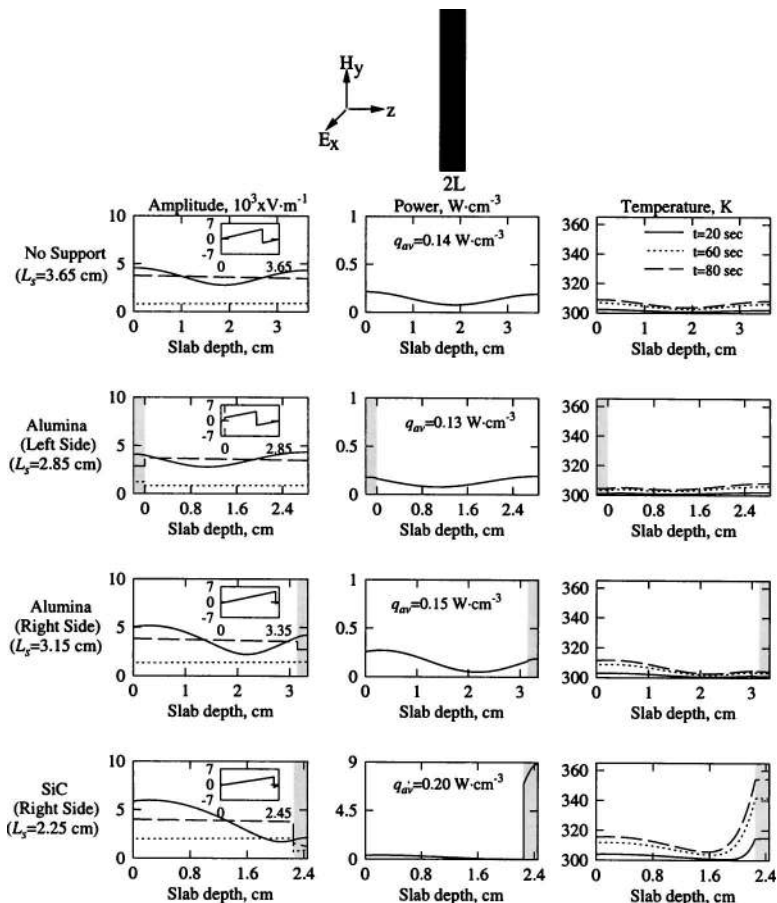


FIG. 7. Amplitudes of electric field ($A_{x,l}, A'_{x,l}, A''_{x,l}$), power distributions, and temperature profiles for oil samples exposed to microwaves from the left face during R_1 mode. The ceramic support thickness = 0.2 cm. - - -, transmitted wave;, reflected wave; —, stationary wave. The shaded regime denotes the ceramic support. The inset shows phase difference ($\delta_{x,l}$) vs z .

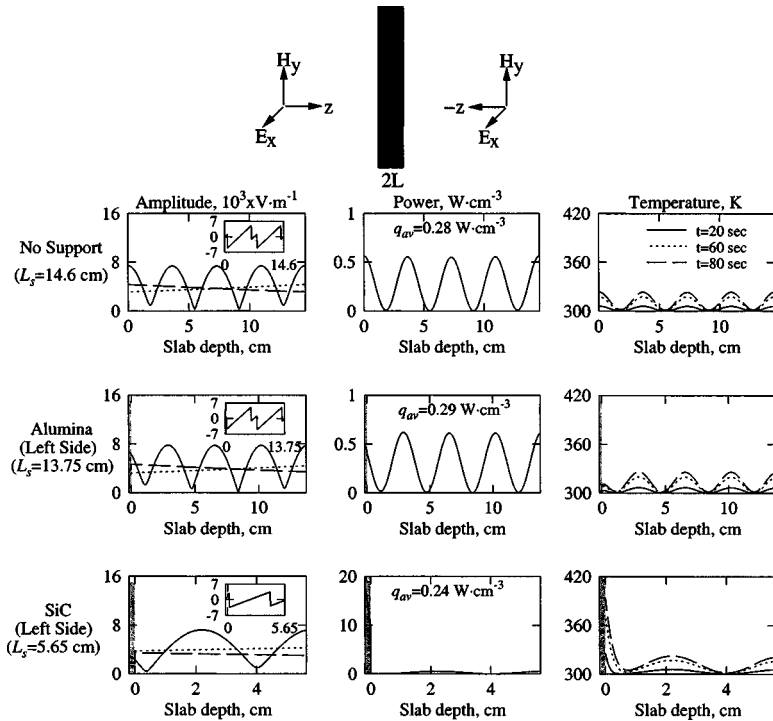


FIG. 8. Amplitudes of electric field ($A_{x,l}, A_{x,l}^t, A_{x,l}^r$), power distributions, and temperature profiles for oil samples exposed to microwaves on both faces during R_2 mode. The ceramic support thickness = 0.2 cm. - - -, transmitted wave; ..., reflected wave; —, stationary wave. The shaded regime denotes the ceramic support. The inset shows phase difference ($\delta_{x,l}$) vs z .

ing 80 s, the temperature near the SiC support is around 354 K, whereas the rest of the sample is at a lower temperature. Hence, the SiC support may not be suitable as the runaway heating would occur when the sample is exposed to MWs for longer duration.

Figure 8 illustrates the amplitude, power, and temperature distributions for oil samples during R_2 mode due to both-sides incidence. As the samples are exposed to MWs

both faces, the transmitted and reflected waves are symmetric with each other, resulting in more power absorption than the one-side incidence case. During R_2 mode, we observe more power peaks within the samples and the spatial distributions of power remain unaffected by the Al_2O_3 support. The SiC support absorbs a considerably greater amount of power, resulting in a very small power deposition within the sample. Note that the average power absorption within a

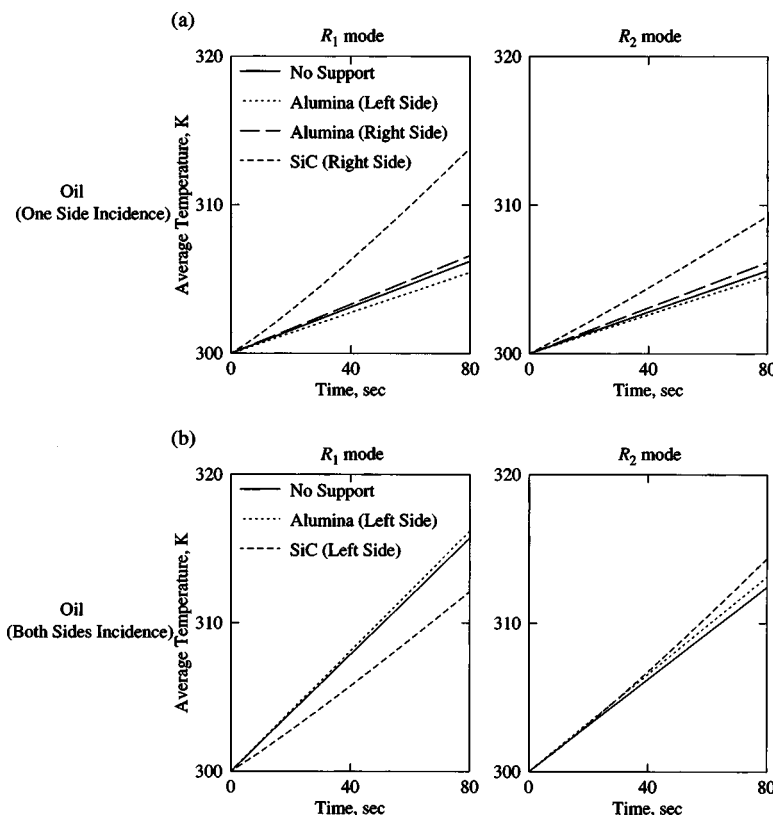


FIG. 9. Average temperature (K) vs sample thickness (cm) for oil samples exposed to microwaves on (a) one face and (b) both faces during R_1 and R_2 modes.

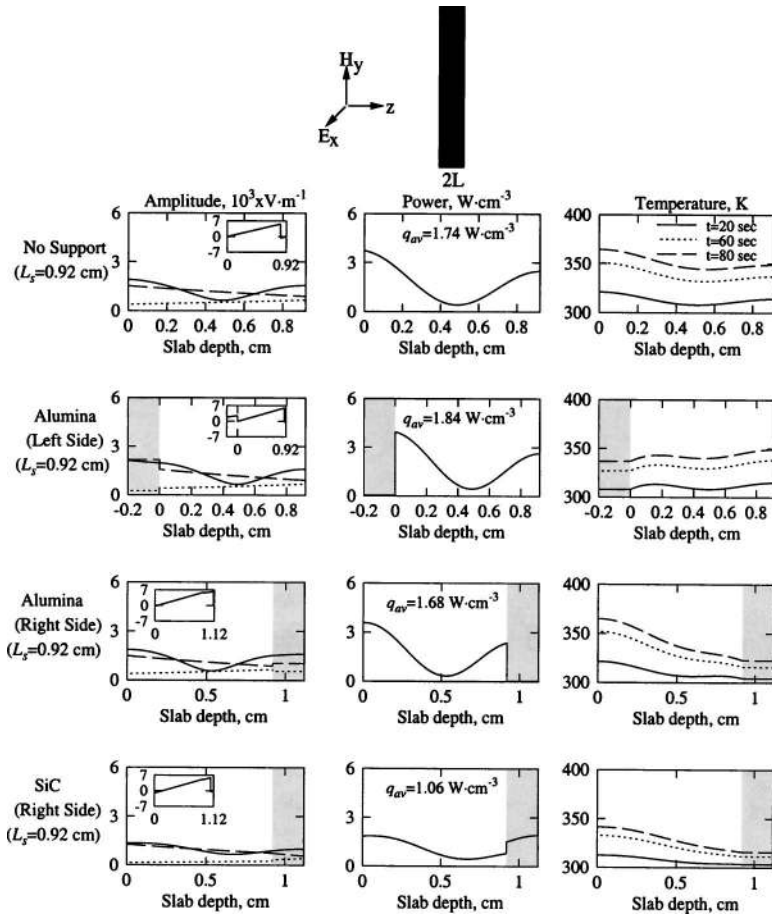


FIG. 10. Amplitudes of electric field ($A_{x,i}, A_{x,j}^i, A_{x,j}^r$), power distributions, and temperature profiles for raw beef samples exposed to microwaves from the left face during R_1 mode. The ceramic support thickness = 0.2 cm. - - -, transmitted wave; reflected wave; —, stationary wave. The shaded regime denotes the ceramic support. The inset shows phase difference ($\delta_{x,i}$) vs z .

sample without a support is around 0.28 W cm^{-3} , whereas the average power is around 0.29 W cm^{-3} for samples with Al_2O_3 supports and that with a SiC support is 0.24 W cm^{-3} . The temperature distribution within the samples follows a similar trend to the power distributions and are not influenced by the Al_2O_3 support. Due to greater power absorption within the SiC support, the runaway heating occurs near the support resulting in a very high temperature, 394 K, whereas the rest of the sample is at lower temperatures. The runaway heating effect is more pronounced in R_2 mode and a similar runaway heating effect with less intensity also occurs during R_1 mode with both-sides incidences (figures are not shown).

Figure 9 illustrates the distribution of average temperature versus time for oil samples with various cases. The average temperature versus time for one-side incidence shows that the heating rate is not much influenced by the Al_2O_3 support and in addition, Al_2O_3 at the right side results in a slightly greater heating rate [Fig. 9(a)]. The greater heating rate is observed due to the SiC support, based on the greater slope of the average temperature versus time plot. It is interesting to note that the greater heating rate does not imply the greater volumetric heating, but the runaway heating effect at a localized regime of the sample near the support, as seen in Fig. 7. We have also shown the heating rates due to R_2 mode, where the SiC support causes the lesser runaway heating effect and the Al_2O_3 supports do not alter the heating rates significantly [Fig. 9(a)].

The average heating rates for both-sides incidence are shown in Fig. 9(b). During R_1 mode, the heating rates with

Al_2O_3 support and without support are almost identical, whereas the less heating rate due to the SiC support is observed. Although the SiC support causes the smaller heating rate, the runaway heating is observed near the support. During R_2 mode, the heating rates are almost identical irrespective of support and the runaway heating effects are observed at the later stages of heating for SiC supports. Note that the greater intensity of runaway heating effects are observed during R_2 mode for both-sides heating, whereas the greater runaway heating effects are observed during R_1 mode for one-side heating. This analysis provides a suitable guideline to choose the optimal thickness of the sample based on the nature of the supports.

D. Microwave power and temperature distributions for raw beef samples

Lastly, we illustrate the electric field, power, and temperature characteristics for a typical food substance, raw beef. The dielectric properties of raw beef as seen in Table I are within the properties of oil and water. Figure 10 illustrates the field, power, and temperature distributions of raw beef for one-side incidence during R_1 mode. As raw beef absorbs less MW power than water, the resonances occur at a greater length than that for water and the resonating length for raw beef is 0.92 cm during R_1 mode with one-side incidence. The spatial distributions of power and temperature follow qualitatively similar to that of water. Note that raw beef with Al_2O_3 support at the exposed side exhibits greater

(a)

MATERIALS	STRATEGY	CONCLUSIVE REMARKS
WATER		<ul style="list-style-type: none"> ● SUPPORT IS AT THE EXPOSED FACE ● SUPPORT DOES NOT INFLUENCE HEATING RATES
		<ul style="list-style-type: none"> ● SUPPORT IS AT THE UNEXPOSED FACE ● LOWER BUT UNIFORM HEATING RATES ARE OBSERVED
OIL		<ul style="list-style-type: none"> ● SUPPORT IS AT THE UNEXPOSED FACE ● SUPPORT DOES NOT INFLUENCE HEATING RATES
		<ul style="list-style-type: none"> ● SUPPORT IS AT THE UNEXPOSED FACE ● LOCALIZED HEATING AND RUN-AWAY EFFECTS ARE OBSERVED

FIG. 11. The heating strategies for various sample-support assembly due to microwave radiations on (a) one face and (b) on both faces. The shaded regime denotes the support.

(b)

MATERIALS	STRATEGY	CONCLUSIVE REMARKS
WATER		<ul style="list-style-type: none"> ● RUNAWAY EFFECT IS OBSERVED WITH Al_2O_3 SUPPORT ● LOWER BUT UNIFORM HEATING RATES ARE OBSERVED WITH SiC SUPPORT
		<ul style="list-style-type: none"> ● Al_2O_3 SUPPORT DOES NOT INFLUENCE HEATING RATES ● LOCALIZED HEATING AND RUN-AWAY EFFECTS ARE OBSERVED WITH SiC SUPPORT

average and spatial power distributions, and we have also observed the similar features for water, where water exhibits greater power with Al_2O_3 support. The temperature distribution is purely governed by thermal diffusion and for raw beef, the spatial temperature near the surface is greater than that for water. At this point, we may highlight that the dielectric response and power characteristics for a material would be derived from the two limits; water and oil and a generalized material invariant analysis would possibly draw a generic guideline which would be useful for efficient thermal processing. The detailed analysis on material invariant analysis is a subject of our ongoing research.

IV. CONCLUSIONS

A detailed analysis on MW power distributions has been illustrated with the distributions of the transmitted and reflected waves for the water and oil samples with Al_2O_3 and SiC supports. In general, the support attached to the unexposed face of the sample corresponds to greater heating rate within samples when the heating is carried out with one-sided MWs incidence. Due to lower dielectric loss, the Al_2O_3 support causes MWs with greater intensity to penetrate, and the sample with greater dielectric loss (water) would heat up rapidly. During both-sides incidence for water samples, it is

observed that the temperature near the unsupported end quickly reaches around 385 K when the sample is kept on Al_2O_3 support. In contrast, the SiC support causes a uniform temperature distribution within the sample. The localized thermal runaway or *hot spot* is more pronounced for water samples with Al_2O_3 support during both-side incidence. Although the SiC sample absorbs a greater amount of power, the uniform heating of water is always found with the SiC support.

We have also carried out investigations for oil samples and due to the lower dielectric loss of oil, the MW power absorption is observed to be low. Therefore, the Al_2O_3 support seems to be a suitable support and oil samples heat uniformly for both one-side and two-sides incidence cases. As the oil sample reflects a significant amount of electric field for both-sides incidence cases, the power absorption within the SiC support is greatly enhanced resulting in a hot spot near the sample face attached with the SiC support. The average heating rate within the oil sample is greater due to the runaway situation and this fact should be considered to decide the suitability of the support. We have also examined the suitability of support for a typical food material.

We feel our analysis is general as we have studied materials with two limits of dielectric response. Our extensive studies would decide the strategy to heat materials and opti-

mal sample-support assembly can be constructed as suggested in Figs. 11(a) and 11(b) for both one-side and both-sides heating. This assembly is useful for uniform plane-wave heating and the heating strategy of any material with intermediate dielectric properties can be deduced from the optimal guideline (Fig. 11).

¹T. Ohlsson and P. O. Risman, *J. Microwave Power* **13**, 303 (1978).

²H. Massoudi, C. H. Durney, P. W. Barber, and M. F. Iskander, *IEEE Trans. Microwave Theory Tech.* **25**, 825 (1979).

³C. M. Weil, *IEEE Trans. Biomed. Eng.* **BME-22**, 468 (1975).

⁴A. K. Datta, *6*, 47 (1990).

⁵K. G. Ayappa, H. T. Davis, G. Crapiste, E. A. Davis, and J. Gordon, *Chem. Eng. Sci.* **46**, 1005 (1991).

⁶K. G. Ayappa, H. T. Davis, E. A. Davis, and J. Gordon, *AIChE J.* **38**,

1577 (1992).

⁷K. G. Ayappa, H. T. Davis, S. A. Barringer, and E. A. Davis, *AIChE J.* **43**, 615 (1997).

⁸K. G. Ayappa, *J. Microwave Power Electromagn. Energy* **34**, 33 (1999).

⁹S. A. Barringer, K. G. Ayappa, E. A. Davis, H. T. Davis, and J. Gordon, *J. Food. Sci.* **60**, 1132 (1995).

¹⁰T. Basak and K. G. Ayappa, *AIChE J.* **43**, 1662 (1997).

¹¹T. Basak and K. G. Ayappa, *AIChE J.* **47**, 835 (2001).

¹²T. Basak and K. G. Ayappa, *Int. J. Heat Mass Transfer* **45**, 4543 (2002).

¹³T. Basak, *Int. J. Heat Mass Transfer* **46**, 4279 (2003).

¹⁴T. Basak, *AIChE J.* **50**, 2659 (2004).

¹⁵A. Chatterjee, T. Basak, and K. G. Ayappa, *AIChE J.* **44**, 2302 (1998).

¹⁶N. Gupta, V. Midha, V. Balakotaiah, and D. J. Economou, *J. Electrochem. Soc.* **146**, 4659 (1999).

¹⁷C. A. Vriezinger, *J. Appl. Phys.* **85**, 3774 (1999).

¹⁸J. N. Reddy, *An Introduction to the Finite Element Method* (McGraw-Hill, New York, 1993).